# Neural Network Method for Detecting and Diagnostics Helicopters Turboshaft Engines Surge at Flight Modes

Serhii Vladov[1], Yurii Shmelov[1], Ruslan Yakovliev[1] and Maryna Petchenko[2]

[1] *Kremenchuk Flight College of Kharkiv National University of Internal Affairs, vul. Peremohy, 17/6, Kremenchuk, Poltavska Oblast, Ukraine, 39605*
[2] *Kharkiv National University of Internal Affairs, L. Landau Avenue, 27, Kharkiv, Ukraine, 61080*

**Abstract**

The work is devoted to the development of a neural network method for diagnostics (monitoring) helicopters turboshaft engines pre-surge status in real time (at helicopter flight mode). The developed method for helicopters turboshaft engines is based on a mathematical model of the time distribution of air pressure in the compressor during the transient process, which is construct on the basis of the classical theory of the movement of liquids and gases, taking into account the features of the thermogas-dynamic flow in the compressor of helicopters turboshaft engines. Diagnostics (monitoring) helicopters turboshaft engines in real time is carried out using a linear neural network with the optimal number of neurons – 10 or more. It is proposed to train a linear neural network on dynamic neurons, which, due to the adjustable smoothing parameter from the range from zero to one, made it possible to obtain an accuracy of 99.99 % of the task being solved. The developed method can serve as one of the blocks of the onboard neural network expert system for the integrated monitoring and operation of helicopters turboshaft engines, which automatically decides on helicopters turboshaft engines operational status at helicopter flight mode and provides the crew with information about the possibility of helicopter further movement.

**Keywords**

Helicopters turboshaft engines, compressor, neural network, training, thermogas-dynamic parameters, diagnostics (monitoring), pre-surge status, signal, pressure, error

## 1. Introduction

At present, a modern aircraft gas turbine engine (GTE) and its control systems are a complex dynamic system. The correctness and safety of the operation of aviation gas turbine engines require constant and continuous monitoring of its parameters, the effectiveness of which significantly depends on the probability of correct recognition of its technical condition, including defects, which directly affects the quality of gas turbine operation control systems, which ultimately determines the efficiency and safety of flights.

One of aircraft GTE leading defects is the stall mode of its operation – surge, which is characterized by various non-stationary phenomena resulting from the loss of stability of the air flow in the compressor. In this case, strong pulsations of the air flow appear, a drop in its pressure, which leads to vibrations of the compressor blades and can cause its destruction. Thus, surge is not allowed during engine operation [1], which indicates the need for its monitoring (diagnostics).

The development of approaches to diagnostics aircraft GTE operational status, including helicopters turboshaft engines (TE), is proceeding in several directions. Much attention is paid to the improvement of algorithmic support, which expands the capabilities of diagnostic models and increases the reliability

The Sixth International Workshop on Computer Modeling and Intelligent Systems (CMIS-2023), May 3, 2023, Zaporizhzhia, Ukraine
EMAIL: ser26101968@gmail.com (S. Vladov); nviddil.klk@gmail.com (Yu. Shmelov); ateu.nv.klk@gmail.com (R. Yakovliev); marinapetcenko@gmail.com (M. Petchenko)
ORCID: 0000-0001-8009-5254 (S. Vladov); 0000-0002-3942-2003 (Yu. Shmelov); 0000-0002-3788-2583 (R. Yakovliev); 0000-0003-1104-5717 (M. Petchenko)

of diagnostics. In [2, 3], the advantages of using artificial intelligence methods over classical diagnostic methods for troubleshooting are shown. It is noted that neural networks are the most effective, since they have high adaptive characteristics and can solve complex problems of classification and pattern recognition. Existing neural network diagnostic methods are limited by the specificity of the tasks being solved, the insufficient development of the theory of their application for TE diagnostics, the lack of universal and formalized approaches, and the imperfection of the methods themselves. In this regard, an urgent scientific and practical task is the development of a neural network method for monitoring (diagnosing) surge (pre-surging state) of TE in helicopter flight conditions, which will significantly improve the safety of helicopter flights.

## 2. Related Works

There are known surge diagnostic methods [4, 5], in which the measured parameters are: gas temperature in front of the compressor turbine, pressure at the inlet and outlet of the compressor, gas generator rotor r.p.m. As is known [6], when a surge occurs, gas temperature in front of the compressor turbine increases, gas generator rotor r.p.m. decreases, and the air pressure behind the compressor sharply decreases relative to the pressure at the inlet to air inlet section. The conclusion about the development of surge in the compressor is made in case of exceeding a predetermined threshold value of the ratio of gas temperature in front of the compressor turbine to gas generator rotor r.p.m.

The disadvantage of the known methods is that the ratio of gas temperature in front of the compressor turbine to gas generator rotor r.p.m. can exceed a predetermined threshold value when the engine operation mode changes, for example, when throttling, on the basis of which a false conclusion can be made about the presence of surge.

An analysis of published works devoted to the use of neural networks for diagnostics the aircraft GTE operational status shows that in [7, 8] the main trends are outlined and the characteristic features of solving the problems of diagnostics aircraft GTE based on neural networks are highlighted.

At the same time, they are mainly devoted to solving particular problems (for example, GTE turbine blades operational status diagnostics [9], forming a space of diagnostics signs of aircraft GTE operational status to build a neural network classifier [10], indirectly measuring the temperature of gases behind the combustion chamber based on neural networks for diagnostics the thermal state of the engine [11]. However, they do not contain instructions on the choice of architecture, structure and training algorithms for the neural network, there is no engineering methodology for designing neural networks in relation to the problems of aircraft GTE operational status diagnostics) of helicopters TE are also missing.

## 3. Methods and Materials

Let $\rho(x, t)$ be the density of the liquid, then applying the law of conservation of mass, we obtain that the rate of change of mass in the volume $V$ must be equal to the mass flow crossing the surface $S$ of the volume $V$ (fig. 1, a). The mass flow through the surface element $dS$ is equal to $-\rho v dS$ [12, 13]:

$$\frac{\partial}{\partial t}\iiint_V \rho d\tau = -\iint_S \rho V dS. \quad (1)$$

Applying the Gauss's-Ostrogradsky's theorem, we arrive at the differential equations for conservation of mass [12, 13]:

$$\frac{\partial \rho}{\partial t} + \nabla \rho V = 0. \quad (2)$$

Similarly, the equation of motion for the medium can be derived from the condition of conservation of pulse. Consider the preservation of the projection of the pulse in the $X$-direction (fig. 1, $b$). The $X$-component of the total pulse in the volume $V$ is $\iiint_V \rho v_x d\tau$. Due to pulse convection and the influence of pressure $p$ in the $X$-direction, the $X$-component of the pulse of the medium in the volume $V$ increases with time ($e_x$ – unit vector in the $X$-direction), i.e., $-\iint_S \left(\rho v_x V + p e_x\right) dS$. Then, from the law of conservation of pulse ($X$-components), we get the equation:

$$\frac{\partial}{\partial t}\iiint_V \rho v_x d\tau = -\iint_S \left(\rho v_x V + p e_x\right) dS. \quad (3)$$

Using the Gauss's-Ostrogradsky's theorem, we obtain:

$$\frac{\partial}{\partial t}\iiint_V \rho v_x d\tau = \iiint_V \nabla\left(\rho v_x V + p e_x\right) d\tau; \quad (4)$$

$$\frac{\partial \rho v_x}{\partial t} + \nabla\left(\rho v_x V + p e_x\right) = 0. \quad (5)$$

Similarly, the equations of motion for the *Y*- and *Z*-directions are obtained. Let's combine these equations and get:

$$\frac{\partial \rho v_x}{\partial t} + \nabla\left(\rho V + pI\right) = 0; \quad (6)$$

where $I$ – unit tensor.

Let's draw two cross-sections at any place of the flow in the gas pipeline, let the distance between them be *dx*.

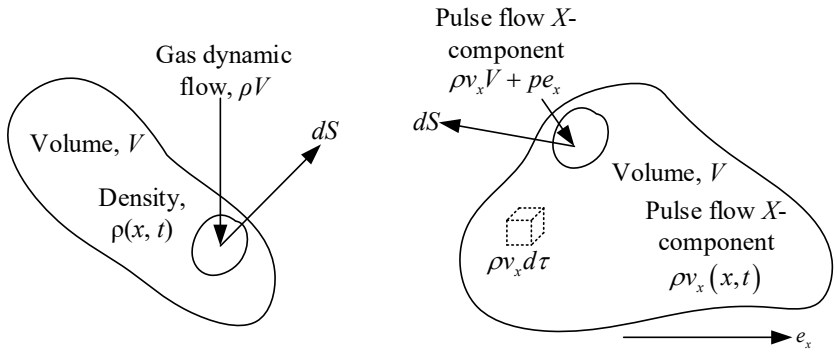


a b

**Figure 1**: Diagram of conservation in the environment: a – mass; b – pulse [12]

Using the pulse theorem, we obtain (fig. 1, *b*):

$$\frac{\partial}{\partial t}\left(\int_f \rho v df dx\right) + \frac{\partial}{\partial x}\left(\int_f \rho v^2 df\right) = -\frac{\partial}{\partial x} fp dx - \tau\chi dx - \gamma f dx \sin\alpha + p\frac{\partial f}{\partial x} = -f\frac{\partial p}{\partial x}dx - \tau\chi dx - \gamma f dx \sin\alpha; \quad (7)$$

where $\rho$ – density; $p$ – average pressure in the section; $f$ – cross-sectional area; $v$ – longitudinal velocity in the cross-sectional element; $t$ – time; $\tau$ – projection of the tangential stress on the pipe wall onto the $X$ axis – flow direction – average over the wetted perimeter; $\chi$ – wetted perimeter; $\gamma$ – gas volume unit weight; $\alpha$ – elevation angle of the $dx$ element axis above the horizon.

We reduce this equation to *dx*, we get:

$$\frac{\partial M}{\partial t} + \frac{\partial f}{\partial x} = -f\frac{\partial p}{\partial x} - \tau\chi - \gamma f dx; \quad (8)$$

where $M$ – flow rate; $I$ – projection on the $X$-axis of the amount of movement of the mass $M$:

$$M = \int_f \rho v df; \quad (9)$$

$$I = \int_f \rho v^2 df. \quad (10)$$

Equation (8) is a general equation that is valid for any gas-dynamic flow in a pipe.

Consider the mass balance entering and leaving the *dx* element, using the continuity theorem, we obtain the equation:

$$\frac{\partial\left(fp\right)}{\partial t} + \frac{\partial M}{\partial x} = 0. \quad (11)$$

In the general case, the quantity $I$ can be given in the form:

$$I = \int_f \rho v^2 df = (1+\beta) f \rho \omega^2 = (1+\beta) M \omega; \tag{12}$$

where $\omega$ – average velocity in the section, $\beta$ – Coriolis correction for the uneven distribution of velocities in the expression of the amount of flow movement due to the average velocity and the average density in the section. As is known, in steady motion for a normal distribution of velocities in a turbulent flow $\beta \approx 0$, in a parabolic distribution $\beta = \frac{1}{3}$. In case of unsteady motion, $\beta$ will naturally be a variable value that depends on the nature of the distribution of velocities in the pipe sections.

Next, we will use the following formula from gas dynamics for the tangential stress $\tau$:

$$\tau = \frac{\lambda}{8} \rho \omega^2; \tag{13}$$

where $\lambda$ – resistance coefficient in the Darcy-Weisbach formula for frictional head loss in the pipe. Its $\lambda$ can always be set knowing the roughness of the pipe and the flow rate.

It is known that $\lambda$ depends on the roughness of the pipe and the mode of movement (Reynolds number). We will accept the following assumption that the resistance characteristics established for stationary movements are preserved for non-stationary ones as well.

Rigorous substantiation of this assumption is quite difficult, although it is confirmed by a rather satisfactory agreement between theory and experience. Using the above remarks, equation (8) will be rewritten in the form:

$$\frac{\partial M}{\partial t} = -S \frac{\partial p}{\partial x} - \frac{\lambda}{8} \rho \omega^2 \chi S \sin\alpha - \frac{\partial}{\partial x}\left((1+\beta) M \omega\right). \tag{14}$$

Since $M = \rho S \omega$, the equation can be simplified:

$$\frac{\partial M}{\partial t} = -S \frac{\partial p}{\partial x} - M \frac{\lambda \omega}{8S} \chi - \gamma S \sin\alpha - \frac{\partial}{\partial x}\left((1+\beta) M \omega\right) = -S \frac{\partial p}{\partial x} - M \frac{\lambda \omega}{8\delta} - \gamma S \sin\alpha - \frac{\partial}{\partial x}\left((1+\beta) M \omega\right); \tag{15}$$

where $\delta$ – hydraulic radius of the section, which is equal to:

$$\delta = \frac{f}{X} = \frac{\pi \frac{d^2}{4}}{\pi d} = \frac{d}{4}; \tag{16}$$

where d is the diameter of the gas pipeline.

Next, let's return to the inseparability equation (11). For gas compression, let's take $S$ = const and use the following formula:

$$c^2 = \frac{\partial p}{\partial \rho}; \tag{17}$$

where $c$ – gas sound speed, from which we obtain, opening the full differentials $dp$ and $d\rho$:

$$\frac{\partial \rho}{\partial t} \partial t + \frac{\partial \rho}{\partial x} \partial x = \frac{1}{c^2} \left( \frac{\partial p}{\partial t} \partial t + \frac{\partial \rho}{\partial x} \partial x \right). \tag{18}$$

Since the increments of dt and dx are arbitrary, it is necessary that $\frac{\partial \rho}{\partial t} = \frac{1}{c^2} \frac{\partial p}{\partial t}$. From here we get the following equation:

$$\frac{\partial (\rho S)}{\partial t} = S \frac{\partial \rho}{\partial t} = \frac{S}{c^2} \frac{\partial p}{\partial t}. \tag{19}$$

As a result, the equation of motion (8) and continuity (11) can be written in the form of the following system:

$$\begin{cases} -S \frac{\partial p}{\partial x} = \frac{\partial M}{\partial t} + M \frac{\lambda \omega}{8\delta} + \gamma S \sin\alpha + \frac{\partial}{\partial x}\left((1+\beta) M \omega\right); \\ -S \frac{\partial p}{\partial t} = c^2 \frac{\partial M}{\partial x}. \end{cases} \tag{20}$$

The system of equations (20) is a system of two differential equations of the first order in partial derivatives of the hyperbolic type, in the general case nonlinear. Dividing both parts of the system by $S$, we get:

$$\begin{cases} -\dfrac{\partial p}{\partial x} = \dfrac{\partial(\rho\omega)}{\partial t} + \dfrac{\lambda}{8\delta} + \gamma\sin\alpha + \dfrac{\partial}{\partial x}\left((1+\beta)M\omega\right); \\ \dfrac{\partial p}{\partial t} = \dfrac{1}{c^2}\dfrac{\partial p}{\partial x} - \dfrac{\partial(\rho\omega)}{\partial t}. \end{cases} \tag{21}$$

Let's simplify the system of equations (20). We will show that in equations (8) and (21) it is possible to neglect the term $\dfrac{\partial I}{\partial x} = \dfrac{\partial}{\partial x}\left((1+\beta)M\omega\right)$.

Let us denote $\sin\alpha = \dfrac{dz}{dx}$, where $z$ – excess of the center of gravity of the pipe section above an arbitrary horizontal plane. It is possible to integrate the first of equations (21) over $x$ from $x_1$ to $x_2$ at a fixed $t$ and present the result in the following form:

$$\left(p_1 + \gamma z_1\right) - \left(p_2 + \gamma z_2\right) = \int_{x_1}^{x_2} \frac{\partial(\rho\omega)}{\partial t}\partial x + \rho\int_{x_1}^{x_2} \frac{\lambda\omega^2}{8\delta}\partial x + \left((1+\beta)\rho\omega^2\right)_2 - \left((1+\beta)\rho\omega^2\right)_1. \tag{22}$$

During the movement of gas with subsonic speed, it is always possible to neglect the dynamic pressure corresponding to the high-speed pressure, as well as to neglect the hydrostatic pressure of the gas due to its low density. It follows that in (21) the last difference $\left((1+\beta)\rho\omega^2\right)_2 - \left((1+\beta)\rho\omega^2\right)_1$ can be omitted, which means $\dfrac{\partial I}{\partial x} = \dfrac{\partial}{\partial x}\left((1+\beta)M\omega\right)$ that the term can be discarded in the first equation of system (20). In the future, under pressure $p$ we mean the sum $p + \gamma z$ and omit the term $\gamma\sin\alpha$. As a result, we will get the following system:

$$\begin{cases} -\dfrac{\partial p}{\partial x} = \dfrac{\partial(\rho\omega)}{\partial t} + \dfrac{\lambda\rho\omega^2}{8\delta}; \\ -\dfrac{\partial p}{\partial t} = c^2\dfrac{\partial(\rho\omega)}{\partial x}. \end{cases} \tag{23}$$

Let's transform system (23) into the form:

$$\begin{cases} -\dfrac{\partial p}{\partial x} = \dfrac{\partial(\rho\omega)}{\partial t} + \dfrac{\lambda\omega}{8\delta}(\rho\omega); \\ -\dfrac{\partial(\rho\omega)}{\partial x} = \dfrac{1}{c^2}\dfrac{\partial p}{\partial t}. \end{cases} \tag{24}$$

Equations known in electrical engineering that describe the change in electric potential along an electric circuit ($d\varphi/dx$) and over time ($d\varphi/dt$) have a similar form, if this electric circuit is composed of elements that have, per unit length, an ohmic resistance of $R_0$, capacity $C_0$ and inductance $L_0$. These equations are known as telegraph equations of a long line and have the form [14, 15]:

$$\begin{cases} -\dfrac{\partial u}{\partial x} = L\dfrac{\partial i}{\partial t} + Ri; \\ -\dfrac{\partial i}{\partial x} = C\dfrac{\partial u}{\partial t}; \end{cases} \tag{25}$$

where $p \to u$, $\rho\omega \to i$, $R = \dfrac{\lambda\omega}{8\delta}$, $L = 1$, $C = \dfrac{1}{c^2}$.

In order to detect surge in the helicopter aircraft TE compressor, an elementary section of its model is considered in the form of a long line, which is a sequential *RCL*-oscillating circuit with a voltage source $U_0$ acting on it. The analysis of free oscillations in a sequential oscillating circuit leads to the solution of a system of two linear differential equations of the first order with constant coefficients of the relative variable state – current in the inductance (blood flow) and the voltage (pressure) on the capacity of the circuit. One of the equations is formed as a result of applying Kirchhoff's second law to the contour:

$$U_L + U_R + U_C - U_0 = 0. \tag{26}$$

The second equation relates the current in the circuit to the voltage on one of the elements:

$$i_L = C\frac{dU_C}{dt}. \tag{27}$$

It is also worth adding two more auxiliary equations describing the voltages on the inductance and resistance:

$$U_R = i_L R; \tag{28}$$

$$U_L = L\frac{di_L}{dt}. \tag{29}$$

Taking into account the above, the system of differential equations according to Kirchhoff's laws has the form:

$$\begin{cases} i_L = C\dfrac{dU_C}{dt}; \\ L\dfrac{di_L}{dt} + i_L R + U_C = U_0. \end{cases} \tag{30}$$

Having expressed from system (30) the derivatives of the voltage on the capacitor and the current in the inductance, we obtain the equation of state:

$$\begin{cases} \dfrac{dU_C}{dt} = i_L \dfrac{1}{C}; \\ \dfrac{di_L}{dt} = -U_C \dfrac{1}{L} - i_L \dfrac{R}{L} + U_0 \dfrac{1}{L} = 0. \end{cases} \tag{31}$$

The unknown state variables in the obtained system of equations (31) are the voltage on the capacitors and the current in the inductance. The matrix of system coefficients (31) in this case has the form $A = \begin{Vmatrix} a_{11} & a_{12} \\ a_{21} & a_{22} \end{Vmatrix}$, where $a_{11} = 0$; $a_{12} = \dfrac{1}{C}$, $a_{21} = -\dfrac{1}{L}$, $a_{22} = -\dfrac{R}{L}$. Therefore

$$A = \begin{Vmatrix} 0 & \dfrac{1}{C} \\ -\dfrac{1}{L} & -\dfrac{R}{L} \end{Vmatrix}. \tag{32}$$

The matrix of free members is determined by the parameters of the active sources in the circuit and has the form:

$$BF = \begin{Vmatrix} 0 \\ U_0 \cdot \dfrac{1}{L} \end{Vmatrix}. \tag{33}$$

The matrix of initial conditions has the form:

$$X(0) = \begin{Vmatrix} U_C(0) \\ i_L(0) \end{Vmatrix} = \begin{Vmatrix} U_0 \\ 0 \end{Vmatrix}. \tag{34}$$

We determine the eigenvalues of matrix A:

$$\begin{vmatrix} -\lambda & \dfrac{1}{C} \\ -\dfrac{1}{L} & -\dfrac{R}{L} - \lambda \end{vmatrix} = 0; \tag{35}$$

$$\lambda^2 + \frac{R}{L}\lambda + \frac{1}{LC} = 0 \Rightarrow \lambda_{1,2} = \frac{-\frac{R}{L} \pm \sqrt{\left(\frac{R}{L}\right)^2 - 4\frac{1}{LC}}}{2} = -\frac{R}{2L} \pm \frac{1}{2}\sqrt{\left(\frac{R}{L}\right)^2 - 4\frac{1}{LC}};$$

$\lambda_{12} = a \pm jb$, because when substituting the model *RCL*-parameters $\left(\dfrac{R}{L}\right)^2 < \dfrac{4}{LC}$, where $a = -\dfrac{R}{2L}$; $b = \dfrac{1}{2}\sqrt{\left|\left(\dfrac{R}{L}\right)^2 - 4 \cdot \dfrac{1}{LC}\right|}$.

$$\lambda_1 - \lambda_2 = (a + jb) - (a - jb) = 2jb.$$

Sylvester's formula is used to calculate $e^{At}$, which has the form:

$$e^{At}=\sum_{k=1}^{n}\frac{\prod_{i=1,i\neq k}^{n}\left(A-\lambda_i\cdot 1\right)}{\prod_{i=1,i\neq k}^{n}\left(\lambda_k-\lambda_i\right)}e^{\lambda_k t};\tag{36}$$

where $1=\begin{Vmatrix}1 & 0\\ 0 & 1\end{Vmatrix}$ – diagonal identity matrix of order $n$ for two states $i_L$ and $U_C$. Then Sylvester's formula takes the form:

$$e^{At}=\frac{A-\lambda_2\cdot 1}{\lambda_1-\lambda_2}e^{\lambda_1 t}-\frac{A-\lambda_1\cdot 1}{\lambda_1-\lambda_2}e^{\lambda_2 t};\tag{37}$$

$$\lambda_2\cdot 1=(a-jb)\cdot\begin{Vmatrix}1 & 0\\ 0 & 1\end{Vmatrix}=\begin{Vmatrix}a-jb & 0\\ 0 & a-jb\end{Vmatrix};$$

$$A-\lambda_2\cdot 1=\begin{Vmatrix}0 & \frac{1}{C}\\ -\frac{1}{L} & -\frac{R}{L}\end{Vmatrix}-\begin{Vmatrix}a-jb & 0\\ 0 & a-jb\end{Vmatrix}=\begin{Vmatrix}-a+jb & \frac{1}{C}\\ -\frac{1}{L} & -\frac{R}{L}-a+jb\end{Vmatrix};$$

$$\lambda_1\cdot 1=(a+jb)\begin{Vmatrix}1 & 0\\ 0 & 1\end{Vmatrix}=\begin{Vmatrix}a+jb & 0\\ 0 & a+jb\end{Vmatrix};$$

$$A-\lambda_1\cdot 1=\begin{Vmatrix}0 & \frac{1}{C}\\ -\frac{1}{L} & -\frac{R}{L}\end{Vmatrix}-\begin{Vmatrix}a+jb & 0\\ 0 & a+jb\end{Vmatrix}=\begin{Vmatrix}-a-jb & \frac{1}{C}\\ -\frac{1}{L} & -\frac{R}{L}-a-jb\end{Vmatrix};$$

$$\frac{A-\lambda_2\cdot 1}{\lambda_1-\lambda_2}=\frac{1}{2jb}\cdot\begin{Vmatrix}-a+jb & \frac{1}{C}\\ -\frac{1}{L} & -\frac{R}{L}-a+jb\end{Vmatrix}=\begin{Vmatrix}-\frac{a}{2jb}+\frac{1}{2} & \frac{1}{2jbC}\\ -\frac{1}{2jbL} & -\frac{R}{2jbL}-\frac{a}{2jb}+\frac{1}{2}\end{Vmatrix};$$

$$\frac{A-\lambda_1\cdot 1}{\lambda_1-\lambda_2}=\frac{1}{2jb}\cdot\begin{Vmatrix}-a-jb & \frac{1}{C}\\ -\frac{1}{L} & -\frac{R}{L}-a-jb\end{Vmatrix}=\begin{Vmatrix}-\frac{a}{2jb}-\frac{1}{2} & \frac{1}{2jbC}\\ -\frac{1}{2jbL} & -\frac{R}{2jbL}-\frac{a}{2jb}-\frac{1}{2}\end{Vmatrix};$$

$$e^{At}=e^{(a+jb)t}\cdot\begin{Vmatrix}-\frac{a}{2jb}+\frac{1}{2} & \frac{1}{2jbC}\\ -\frac{1}{2jbL} & -\frac{R}{2jbL}-\frac{a}{2jb}+\frac{1}{2}\end{Vmatrix}-e^{(a-jb)\cdot}\cdot\begin{Vmatrix}-\frac{a}{2jb}-\frac{1}{2} & \frac{1}{2jbC}\\ -\frac{1}{2jbL} & -\frac{R}{2j\cdot bL}-\frac{a}{2jb}-\frac{1}{2}\end{Vmatrix}.\tag{38}$$

To calculate the voltage on the capacitor and the current in the inductance, the state equations are solved in matrix form:

$$X(t)=e^{At}\cdot X(0)+\int_0^t e^{A(t-\tau)}\cdot BFd\tau=e^{(a+jb)t}\cdot\begin{Vmatrix}-\frac{a}{2jb}+\frac{1}{2} & \frac{1}{2jbC}\\ -\frac{1}{2jbL} & -\frac{R}{2jbL}-\frac{a}{2jb}+\frac{1}{2}\end{Vmatrix}\cdot\begin{Vmatrix}U_0\\ 0\end{Vmatrix}-e^{(a-jb)t}\times$$

$$\times\begin{Vmatrix}-\frac{a}{2jb}-\frac{1}{2} & \frac{1}{2jbC}\\ -\frac{1}{2jbL} & -\frac{R}{2jbL}-\frac{a}{2jb}-\frac{1}{2}\end{Vmatrix}\cdot\begin{Vmatrix}U_0\\ 0\end{Vmatrix}+\int_0^t\left(e^{(a+jb)(t-\tau)}\cdot\begin{Vmatrix}-\frac{a}{2jb}+\frac{1}{2} & \frac{1}{2jbC}\\ -\frac{1}{2jbL} & -\frac{R}{2jbL}-\frac{a}{2jb}+\frac{1}{2}\end{Vmatrix}\cdot\begin{Vmatrix}0\\ U_0\frac{1}{L}\end{Vmatrix}-\right.$$

$$-e^{(a-jb)(t-\tau)}\cdot\begin{Vmatrix}-\frac{a}{2jb}-\frac{1}{2} & \frac{1}{2jbC}\\ -\frac{1}{2jbL} & -\frac{R}{2jbL}-\frac{a}{2jb}-\frac{1}{2}\end{Vmatrix}\cdot\begin{Vmatrix}0\\ U_0\frac{1}{L}\end{Vmatrix}\Bigg)d\tau=e^{(a+jb)t}\cdot\begin{Vmatrix}-U_0\left(\frac{a}{2jb}-\frac{1}{2}\right)\\ -\frac{U_0}{2jbL}\end{Vmatrix}-e^{(a-jb)t}\times$$

$$\times\begin{Vmatrix}-U_0\left(\frac{a}{2jb}+\frac{1}{2}\right)\\ -\frac{U_0}{2jbL}\end{Vmatrix}+\int_0^t\left(e^{(a+jb)(t-\tau)}\cdot\begin{Vmatrix}\frac{U_0}{2jbLC}\\ -\frac{U_0\left(\frac{a}{2jb}+\frac{R}{2jbL}-\frac{1}{2}\right)}{L}\end{Vmatrix}-e^{(a-jb)(t-\tau)}\cdot\begin{Vmatrix}\frac{U_0}{2jbLC}\\ -\frac{U_0\left(\frac{a}{2jb}+\frac{R}{2jbL}+\frac{1}{2}\right)}{L}\end{Vmatrix}\right)d\tau.$$

Taking into account $L = 1$, the voltage on the capacitor is calculated as follows:

$$U_C(t)=-e^{(a+jb)t}U_0\left(\frac{a}{2jb}-\frac{1}{2}\right)+e^{(a-jb)t}U_0\left(\frac{a}{2jb}+\frac{1}{2}\right)+\int_0^t\left(\frac{U_0}{2jbC}\cdot e^{(a+jb)(t-\tau)}-\frac{U_0}{2jbC}e^{(a-jb)(t-\tau)}\right)d\tau=$$

$$-e^{(a+jb)t}U_0\left(\frac{a}{2jb}-\frac{1}{2}\right)+e^{(a-jb)t}U_0\left(\frac{a}{2jb}+\frac{1}{2}\right)+\frac{U_0}{2jbC}\left(\frac{e^{at+jbt}-1}{a+jb}-\frac{e^{at-jbt}-1}{a-jb}\right)=-e^{\left(-\frac{R}{2}+j\frac{1}{2}\sqrt{\left|R^2-\frac{4}{C}\right|}\right)t}\times$$

$$\times U_0\left(\frac{-\frac{R}{2}}{j\sqrt{\left|R^2-\frac{4}{C}\right|}}-\frac{1}{2}\right)+e^{\left(-\frac{R}{2}-j\frac{1}{2}\sqrt{\left|R^2-\frac{4}{C}\right|}\right)t}\cdot U_0\left(\frac{-\frac{R}{2}}{j\sqrt{\left|R^2-\frac{4}{C}\right|}}+\frac{1}{2}\right)+\frac{U_0}{jC\sqrt{\left|R^2-\frac{4}{C}\right|}}\left(\frac{e^{\left(-\frac{R}{L}+j\frac{1}{2}\sqrt{\left|R^2-\frac{4}{C}\right|}\right)\cdot t}-1}{-\frac{R}{2}+j\frac{1}{2}\sqrt{\left|R^2-\frac{4}{C}\right|}}-\right.$$

$$\left.-\frac{e^{\left(-\frac{R}{2}-j\cdot\frac{1}{2}\cdot\sqrt{\left|R^2-\frac{4}{C}\right|}\right)\cdot t}-1}{-\frac{R}{2}-j\cdot\frac{1}{2}\cdot\sqrt{\left|R^2-\frac{4}{C}\right|}}\right). \tag{39}$$

Expression (39) describes the pressure distribution in the compressor over time. Since surge is characterized by a sharp change in pressure at the inlet and outlet of the compressor, an increase in the gas temperature in front of the compressor turbine and a decrease in gas generator rotor r.p.m., therefore, it is advisable to use expression (39) to monitoring the pre-surge engine status.

Since the air flow turbulence phenomenon takes place in the compressor of helicopters TE [16, 17], we assume that the useful signal $U_C(t)$ is mixed with noise $\delta_0$ that is not correlated with it. The signal $\delta$ is set, it is not correlated with $U_C$, but correlates in an unknown way with the interference signal $\delta_0$. It is assumed that $U_C$, $\delta_0$ and $\delta$ are statistically stationary, and their average values are equal to zero. The task of the neural network is to process the signal $\delta$ in such a way that the signal $y$ at the output of the network is as close as possible to the noise signal $\delta_0$. The error signal $\varepsilon$ is determined according to the expression:

$$\varepsilon = U_C + \delta_0 - y. \tag{40}$$

The objective function is presented in the form of the expected value $E$ of the quadratic error:

$$Z=\frac{1}{2}E\left[\Delta^2\right]=\frac{1}{2}E\left[U_C^2+\left(\delta_0-y\right)^2+2\delta\left(\delta_0-y\right)\right]. \tag{41}$$

If we take into account that the signal $U_C$ does not correlate with the noise signal, then the expected value $E\left[\delta\left(\delta_0-y\right)\right]=0$, and the objective function is simplified to the expression

$$Z=\frac{1}{2}\left(E\left[U_C^2\right]+E\left[\left(\delta_0-y\right)^2\right]\right). \tag{42}$$

Since the filter does not change the signal $U_C$, minimization of the objective function of the error Z is ensured by selecting its parameters in such a way that the value of $E\left[\left(\delta_0-y\right)^2\right]\to\min$. Thus, reaching the minimum of the objective function $Z$ means the best adaptation of the value of $y$ to the

noise $\delta_0$. The minimum possible value $x = E\left[U_C^2\right]$ for which $y = \delta_0$. In this case, the output signal $\varepsilon$ corresponds to the useful signal $U_C$ completely denoised.

In the task of monitoring helicopters TE pre-surge status, the input signal and the objective function coincide, that is, the training error of the neural network, which must be minimized, is determined according to the expression:

$$E(w) = \frac{1}{N}\sum_{n=1}^{N} e(n)^2 = \frac{1}{N}\sum_{n=1}^{N}\left(d(n) - y(n)\right)^2. \tag{43}$$

To solve the task of monitoring helicopters TE pre-surge status, we consider the use of a linear neural network (fig. 2), which consists of $K$ neurons located in one layer and connected to **R** inputs through the weight matrix **W**.

For a given network and the corresponding set of input and target vectors, it is possible to calculate the network output vector and form the difference between the output vector and the target vector, which will determine some error [18]. In the training process, it is required to find such values of weights and biases so that the sum of the squares of the corresponding errors is minimal. A supervised training procedure is proposed that uses a training set of the form $\{p_1,t_1\},\{p_2,t_2\},...,\{p_K,t_K\}$, where $p_1$, $p_2$, …, $p_K$ – neural network inputs, $t_1$, $t_2$, …, $t_K$ – corresponding target outputs. It is required to minimize the following mean square error function:

$$E(k) = \frac{1}{K}\sum_{k=1}^{K}\left(e(k)\right)^2 = \frac{1}{K}\sum_{k=1}^{M}\left(t(k) - a(k)\right)^2. \tag{44}$$

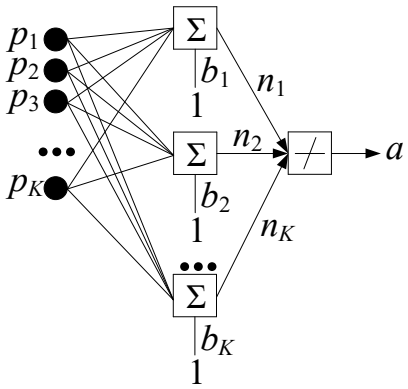


**Figure 2**: Neural network structure

If signal values at different time intervals are used as an input vector for a neural network, then the linear network is a linear adaptive filter with a finite impulse response. The difference equation describing the communication between the input and output signals of such a filter has the form [20]:

$$y(n) = b_0 x(n) + b_1 x(n-1) + ... + b_P x(n-P); \tag{45}$$

where $P$ – filter order; $x(n)$ – input signal; $y(n)$ – output signal; $b_i$ – filter coefficients.

For a linear neural network, a recurrent training least squares rule is used; it minimizes the mean value of the sum of squares of training errors [19]. You can estimate the total standard error using the standard error of one iteration.

It is known that a standard static neuron implements a non-linear mapping [21, 22]:

$$x_j^{[k+1]} = \psi_j^{[1]} u_j^{[k+1]} = \psi_j^{[1]} \sum_{i=0}^{n^{[1]}} u_{j,i}^{[k+1]} = \psi_j^{[1]} \sum_{i=0}^{n^{[1]}} w_{j,i}^{[1]} x_i^{[1]}; \tag{46}$$

the synaptic weights $w_{j,i}^{[1]}$ of which are subject to refinement in the process of training the neural network.

A nonlinear mapping implemented by a dynamic neuron can be written as:

$$x_j^{[k+1]}(k) = \psi_j^{[1]} u_j^{[k+1]}(k) = \psi_j^{[1]} \sum_{i=0}^{n^{[1]}} u_{j,i}^{[k+1]}(k) = \psi_j^{[1]} \sum_{i=0}^{n^{[1]}} w_{j,i}^{[1]} x_i^{[1]}(k). \tag{47}$$

To train neural networks on dynamic neurons, according to [23], a gradient procedure is used – the back propagation of errors in time.

According to [23], the one-step training criterion is defined as:

$$J(k)=\frac{\left\|e(k)\right\|^2}{2}=\frac{\left\|d(k)-N\left(x^{[1]},w^{[1]},...,w^{[K]}\right)\right\|^2}{2}=\frac{\left\|d(k)-\hat{x}(k)\right\|^2}{2}; \quad (48)$$

where $d(k)$ is the training signal, which in the problem being solved is taken as the current value $x(k)$, that is, the signal $U_C(k)$.

According to [23], the procedure for minimizing the training criterion is:

$$w_{j,i}^{[1]}(k+1)=w_{j,i}^{[1]}(k)-\gamma^{[1]}(k)\frac{\partial J(k)}{\partial u_j^{[1]}(k+1)}\nabla_{w_{j,i}^{[1]}}u_j^{[1]}(k); \quad (49)$$

where $\gamma^{[1]}(k)$ – parameter that determines the training convergence rate.

According to [23], local training error is defined as:

$$\frac{\partial J(k)}{\partial u_j^{[1]}(k+1)}=\delta_j^{[1]}(k). \quad (50)$$

The procedure for setting the neurons of the output layer is [23]:

$$w_{j,i}^{[K]}(k+1)=w_{j,i}^{[K]}(k)+\gamma^{[K]}(k)e_j(k)\psi_j'^{[K]}u_j^{[K]}(k)x_i^{[K]}(k)=w_{j,i}^{[K]}(k)+\gamma^{[K]}(k)e_j(k)J_i^{[K]}(k). \quad (51)$$

The local training error for the hidden layers of the neural network is [23]:

$$\delta_j^{[1]}(k)=\frac{\partial J(k)}{\partial u_j^{[1]}(k+1)}=\sum_{q=1}^{n_{k+1}}\sum_{t=k}^{n_A^{[1]}+k}\delta_q^{[k+1]}(t)\frac{\partial u_q^{[k+1]}(t)}{\partial u_j^{[1]}(k)}=\psi_j'^{[k-1]}u_j^{[1]}(k)\sum_{q=1}^{n_{k+1}}\sum_{t=k}^{n_A^{[1]}+k}\delta_q^{[k+1]}(t)\frac{\partial u_{j,q}^{[k+1]}(t)}{\partial x_j^{[1]}(k)}. \quad (52)$$

An adaptive procedure is written as [23]:

$$w_{j,i}^{[1]}(k+1)=w_{j,i}^{[1]}(k)+\frac{e_j^{[1]}(k)J_i^{[1]}(k)}{\beta+\left\|J_i^{[1]}(k)\right\|^2}; \quad (53)$$

where $\beta > 0$ – regularizing parameter.

The procedure for setting up the training process in hidden layers is optimized for speed. Thus, taking into account [23], the modified neural network training method has the form:

$$\begin{cases} w_{j,i}^{[1]}(k+1)=w_{j,i}^{[1]}(k)+\dfrac{e_j^{[1]}(k)J_i^{[1]}(k)}{\beta_i^{[1]}(k)}; \\ \beta_i^{[1]}(k+1)=\alpha\beta_i^{[1]}(k)+\left\|J_i^{[1]}(k)\right\|^2; \end{cases} \quad (54)$$

where $0 \le \alpha \le 1$ – smoothing parameter, which is selected within a given interval for the most efficient value of the neural network.

A distinctive feature of the modified neural network training method from the method proposed in [23] is the use of a custom smoothing parameter $\alpha$. The proper choice of the value of the smoothing parameter $\alpha$ is critical to the performance of the neural network. Note that the value of $\alpha$ affects the quality of restoring the output signal of the neural network. The method has been modified in order to impart smoothing properties necessary for processing "noisy" signals, such as $U_C(t)$.

However, a significant limitation [23] is the lack of a description of the criterion for choosing the smoothing parameter. In this paper, we propose to select the smoothing parameter for the task diagnostics (monitoring) helicopters TE pre-surge status in real time.

## 4. Experiment

In the experimental work, the signal $U_C(t)$ obtained according to (39) is used and analyzed for the TV3-117 TE, which is part of the power plant of the Mi-8MTV helicopter, according to the data obtained on board the helicopter during the flight [24] (table 1).

**Table 1**
Transfer function coefficient values

| Number | $\lambda$ | $\omega$ | $\delta$ | $c$ |
|---|---|---|---|---|
| 1 | 0.985 | 0.992 | 0.973 | 0.999 |
| 2 | 0.989 | 0.991 | 0.976 | 0.999 |
| 3 | 0.987 | 0.996 | 0.977 | 0.999 |
| 4 | 0.974 | 0.983 | 0.971 | 0.999 |
| 5 | 0.977 | 0.982 | 0.968 | 0.999 |
| 6 | 0.972 | 0.987 | 0.978 | 0.999 |
| 7 | 0.981 | 0.988 | 0.973 | 0.999 |
| 8 | 0.983 | 0.993 | 0.975 | 0.999 |
| 9 | 0.992 | 0.990 | 0.977 | 0.999 |
| ... | ... | ... | ... | ... |
| 256 | 0.985 | 0.991 | 0.974 | 0.999 |

To conduct experimental researches (test example), the Matlab application package was used. The diagram of the dependence of the signal amplitude on time for the signal under study is shown in fig. 3, where a – signal with noise taken into account, b – simulated area of a sharp pressure drops [12]. On fig. 3 input signal values are given in absolute units. Fig. 4 shows a diagram of the probability distribution for a noise signal, where a – signal probability distribution (Gaussian form), b – signal correlation function.

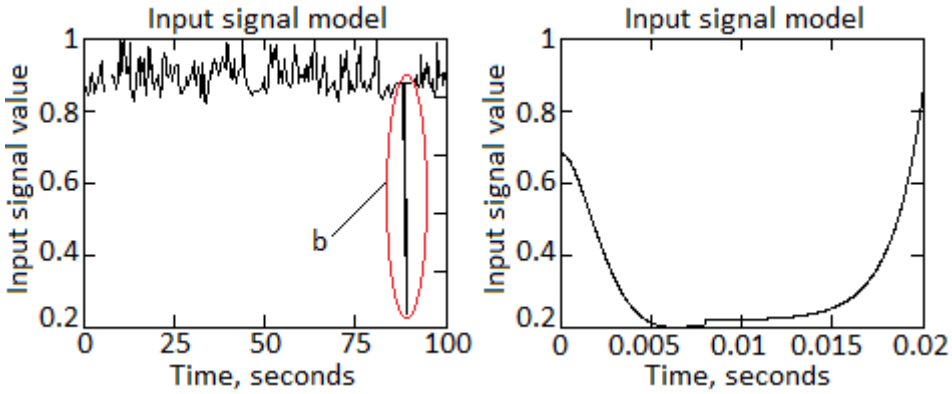


a b

**Figure 3**: Input signal diagram: a – signal with noise taken into account; b – sudden pressure drop area [12]

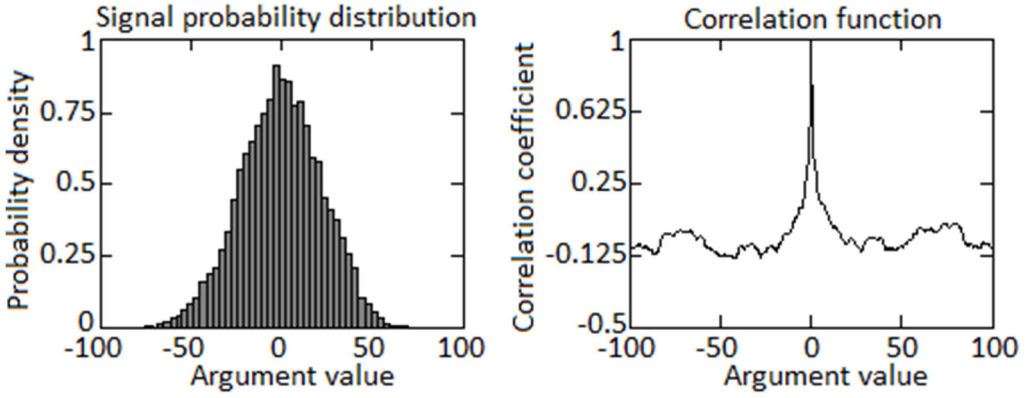


a b

**Figure 4**: Input signal diagram: a – signal probability distribution; b – signal correlation function

To form the training and test subsets, cross-validation [25] was used to estimate the values of TV3-117 TE parameters, the results of which are shown in fig. 5.

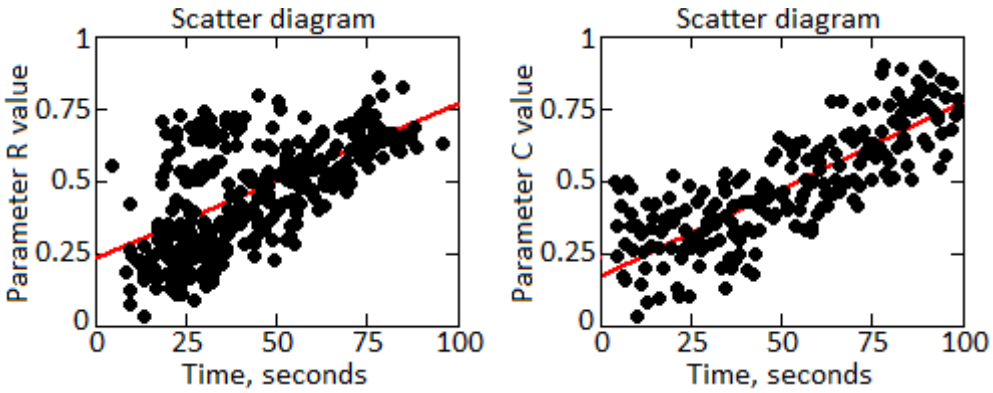


a b

**Figure 5**: Scatter diagram of input parameters: a – parameter *R*; b – parameter *C*

As the input signal $U_C$ for the neural network (fig. 2), a sequential sampling of the values of the fragment of the noise signal was used. The delay line consists of 10 blocks, that is, a sequence of $U_C/10$ values is fed to the input of each neuron. The output signal of the network was the sum of the output signals of each of the neurons. The network had one layer of neurons with a linear activation function. The number of neuron inputs was equal to the sample length of the studied signal. The initial weights of neurons were initiated by random values, and the bias was chosen to be the same and equal to $b = 0.027$.

A supervised training algorithm was used to train the network, and a sequence of input signal values was used as the target vector. The absolute network training error is calculated according to (43): $E(n)=\frac{1}{N}\sum_{n=1}^{N}\left(e(n)\right)^2=\frac{1}{N}\sum_{k=1}^{M}\left(Y(n)-U_C(n)\right)^2$, where $Y(n)$ – output signal of the network, $U_C(n)$ – neural network input signal values, $N$ – input vector dimension. The relative error of the output signal is determined according to the expression:

$$\delta E=\frac{E(n)}{\sigma^2}; \tag{55}$$

where $\sigma^2 = 0.00028$ – neural network input signal variance.

The neural network was trained on a sample of 100 input values of the $U_C$ signal, which is $3T_{cor}$. The signal was applied to the input of each of 10 neurons with 10 signal values on the segment [0; 100], the neural network training rate was chosen as 0.1 (this value was chosen according to the same principles as the number of neurons). Training was carried out at different values of training cycles (depending on the experiment, values from 1 to 100 were used). In order to establish the representativeness of the training and test samples, a cluster analysis [26] of the initial data was carried out (table 1), during which eight classes were identified (fig. 6, a). After the randomization procedure, the actual training (control) and test samples were selected (in a ratio of 2:1, that is, 67 % and 33 %). The process of clustering the training (fig. 6, b) and test samples shows that they, like the original sample, contain eight classes each. The distances between the clusters practically coincide in each of the considered samples, therefore, the training and test samples are representative.

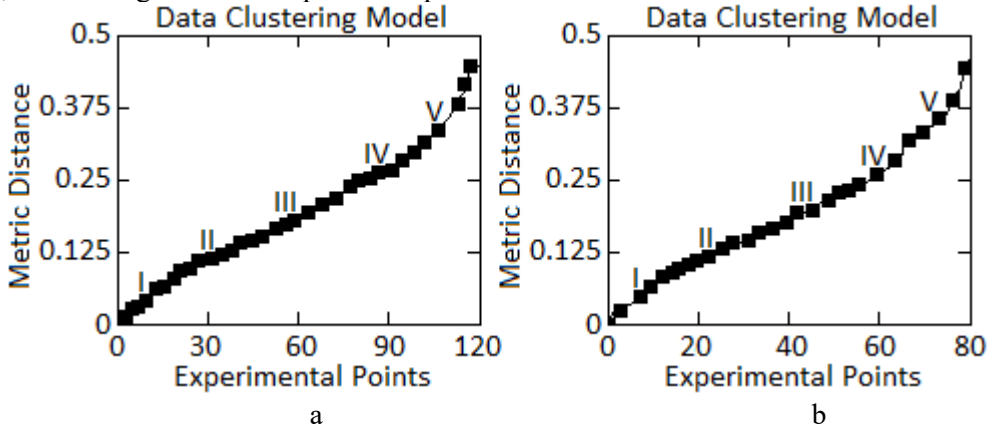


a b

**Figure 6**: Clustering results: a – initial experimental sample (I…V – classes); b – training sample

The assessment of the homogeneity of the training and test samples is carried out using the Fisher-Pearson $\chi^2$ criterion [27] with $r-k-1$ degrees of freedom:

$$\chi^2 = \min_{\theta} \sum_{i=1}^{r} \left( \frac{m_i - np_i(\theta)}{np_i(\theta)} \right); \tag{56}$$

where $\theta$ – maximum likelihood estimate found from the frequencies $m_1, \ldots, m_r$; $n$ – number of elements in the sample; $p_i(\theta)$ – probabilities of elementary outcomes up to some indeterminate $k$-dimensional parameter $\theta$.

The above-mentioned statistics $\chi 2$ permits, under the above assumptions, to check the hypothesis about the representability of sample variances and covariance of factors contained in the statistical model. The field of hypothesis acceptance is $\chi^2 \le \chi_{n-m,\alpha}$, where $\alpha$ – significance level of the criterion.

The results of calculations in accordance with (56) are in table 2.

**Table 2**

Part of the training sample during the helicopters TE operation (on the example of TV3-117 TE)

| Number | $P(\lambda)$ | $P(\omega)$ | $P(\delta)$ | $P(c)$ |
|---|---|---|---|---|
| 1 | 0.739 | 0.784 | 0.798 | 0.989 |
| 2 | 0.742 | 0.783 | 0.800 | 0.989 |
| 3 | 0.740 | 0.787 | 0.801 | 0.989 |
| 4 | 0.731 | 0.776 | 0.796 | 0.989 |
| 5 | 0.733 | 0.779 | 0.794 | 0.989 |
| 6 | 0.729 | 0.780 | 0.802 | 0.989 |
| 7 | 0.736 | 0.781 | 0.798 | 0.989 |
| 8 | 0.738 | 0.784 | 0.800 | 0.989 |
| 9 | 0.744 | 0.782 | 0.801 | 0.989 |
| ... | ... | ... | ... | ... |
| 256 | 0.739 | 0.783 | 0.799 | 0.989 |

Calculation of the $\chi 2$ value based on the observed frequencies $m_1, \ldots, m_r$ (summing line by line the probabilities of the outcomes of each measured value) and comparing it with the critical values of the distribution $\chi 2$ with the number of degrees of freedom $r - k - 1$. In this article, with the number of degrees of freedom $r - k - 1 = 13$ and $\alpha = 0.05$, the random variable $\chi 2 = 3.588$ did not exceed the critical value from table 4 is 22.362, which means that the hypothesis of the normal distribution law can be accepted and the samples are homogeneous.

## 5. Results

Table 3 shows the results of the neural network operation for various values of the smoothing parameter. The network teacher is the value 0.989, which is the average value of the input sample (table 1).

**Table 3**

The results of determining the smoothing parameter

| $\alpha = 0.1$ | $\alpha = 0.2$ | $\alpha = 0.3$ | $\alpha = 0.4$ | $\alpha = 0.5$ | $\alpha = 0.6$ | $\alpha = 0.7$ | $\alpha = 0.8$ | $\alpha = 0.9$ | $\alpha = 1.0$ |
|---|---|---|---|---|---|---|---|---|---|
| 0.9951 | 0.9945 | 0.9934 | 0.9926 | 0.9921 | 0.9915 | 0.9912 | 0.9889 | 0.9873 | 0.9862 |

The results show that at $\alpha = 0.8$, the predicted value is closest to the teacher by 99.99 %.

The neural network training error depending on the number of training cycles is illustrated by the diagram in fig. 7 (a – diagram corresponds to 5 training cycles, b – diagram corresponds to training cycles), which show the input and output signals of the neural network resulting from training, where 1 – initial signal $U_C$, 2 – neural network output signal.

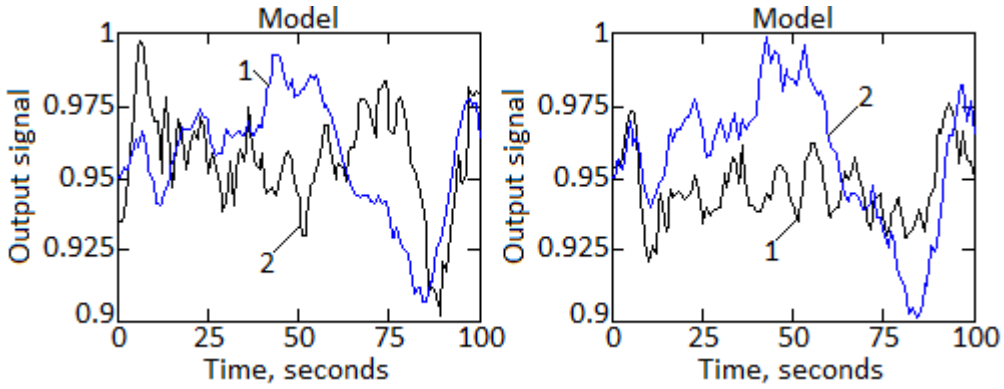


a b

**Figure 7**: Diagram of neural network output and signal versus time

Fig. 7, a corresponds to an absolute error of 0.004717 and a neural network training time of 1.5 seconds. Fig. 7, b corresponds to an absolute error of 0.000000638 and a neural network training time of 11.8 seconds. A diagram of the dependence of the neural network training error on the number of training cycles is shown in fig. 8, from which it can be seen that the error decreases with an increase in the number of training cycles approximately according to a linear law. The training quality of the neural network was also assessed using regression analysis of neural network input and output signals.

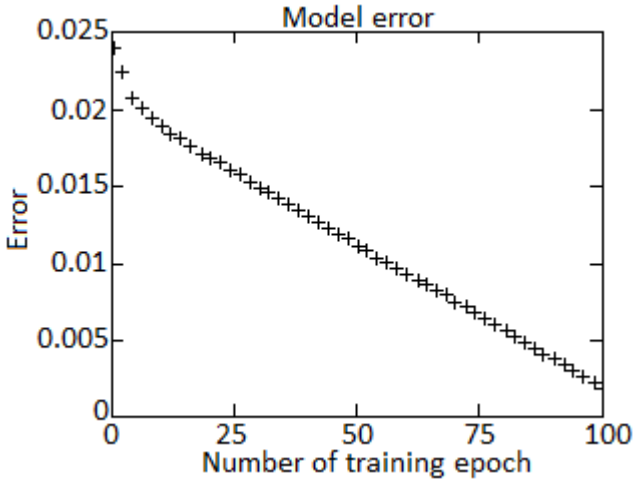


**Figure 8**: Diagram of neural network training error dependence on the number of cycles

The dependence of neural network training error on the number of neurons is shown in fig. 9, from which it can be seen that the training error decreases with an increase in the number of neurons.

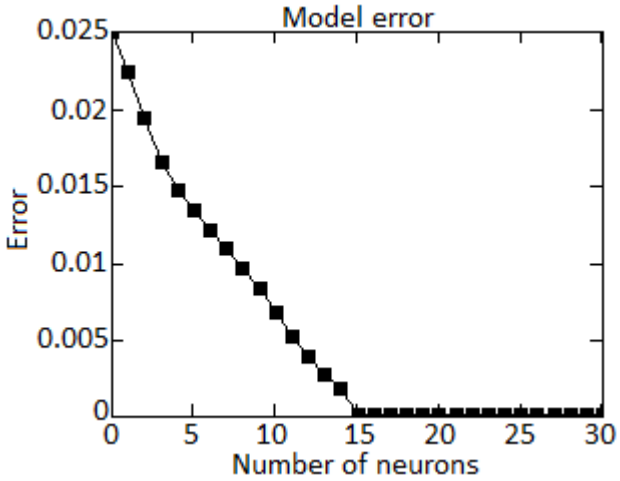


**Figure 9**: Neural network training error versus number of neurons diagram

When the number of neurons is more than 15, it decreases to a minimum and ceases to change. At the same time, the training time increases from 3 seconds with 3 neurons to 150 seconds with 15 neurons. In further experiments, to increase the training rate, the number of neurons was chosen to be 10.

To check the independence of the residuals, the Durbin-Watson test, the autocorrelation function, etc. are usually used. [28, 29]. To check the normality of the distribution of residuals, a plot of the normal distribution of residuals was constructed, that is, the correlation field between the target vector $U_C$ (input signal values at each point) and the output of the neural network $Z$ after 50 training cycles (fig. 9). It can be seen that the distribution is normal – almost all observations follow the line, the points are grouped near the straight line in fig. 10. A high value of the correlation coefficient $R$ = 0.999 indicates that the neural network training algorithm was chosen correctly.

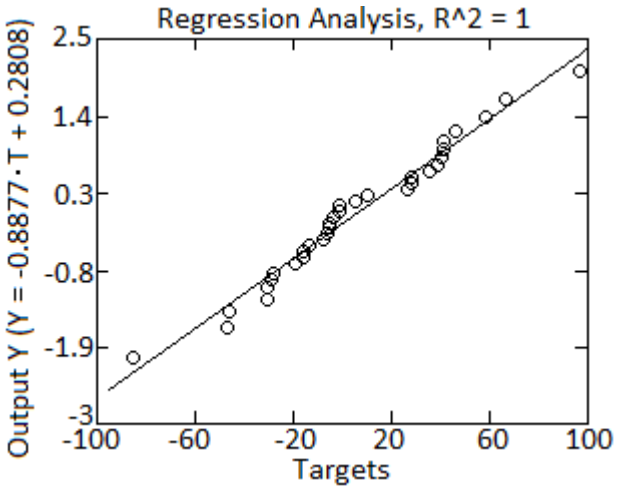


**Figure 10**: Normal distribution diagram of residuals (Regression Analysis)

## 6. Discussions

The neural network input signal and neural network simulated output signal after training on a sample with a length of 100 reports ($3T_{cor}$) are shown in fig. 11, where 1 – initial signal, 2 neural network – output signal. Fig. 11, a show the signals immediately after training the neural network, fig. 11, b – after a time interval corresponding to 30 input noise correlation times. From fig. 11 it can be seen that, despite the increase in the time interval for diagnosing (monitoring) the neural network, the developed method makes it possible to determine the helicopters TE pre-surge status.

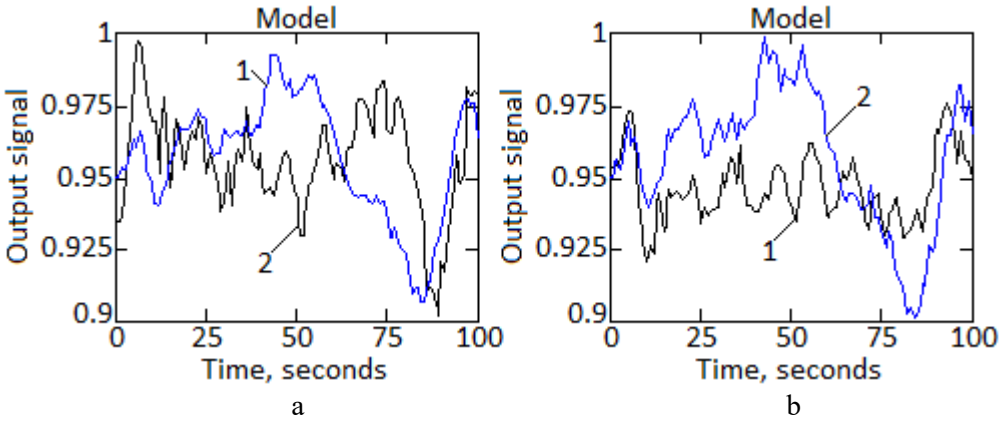


a b

**Figure 11**: Diagram of research of TV3-117 TE pre-surge status

Fig. 12 shows the results of determining the error in diagnostics (monitoring) of helicopters TE pre-surge status using the developed neural network, where 1 – initial signal $U_C$ error, 2 – upper error limit, 3 – lower error limit, 4 – trend line.

As can be seen from fig. 12, a, the maximum error in diagnostics (monitoring) of helicopters TE pre-surge status does not exceed 0.3 %, which indicates an accuracy of > 99 % of the developed method.

To reduce the training time, the neural network went through 3 training cycles, and the error was measured at a prediction time of $300T_{cor}$, while the diagnostics (monitoring) error remained unchanged. From fig. 12, b it can be seen that with an increase in the length of the input vector, the relative network training error decreases significantly. The training time increases with the length of the input vector: with a length equal to $3T_{co}$, the training time is 3.5 seconds, and with a length of 100 correlation times it increases to 60 seconds.

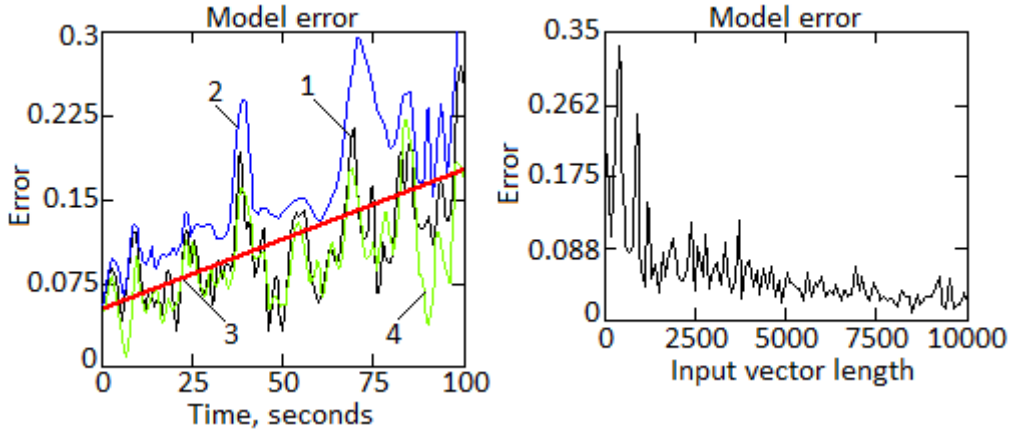


a b

**Figure 12**: Diagram for determining the diagnostics (monitoring) error: a – diagram of the dependence of the diagnostics (monitoring) error on time; b – diagram of diagnostics (monitoring) error versus input vector length

Fig. 13 shows the results of modeling helicopters TE surge status.

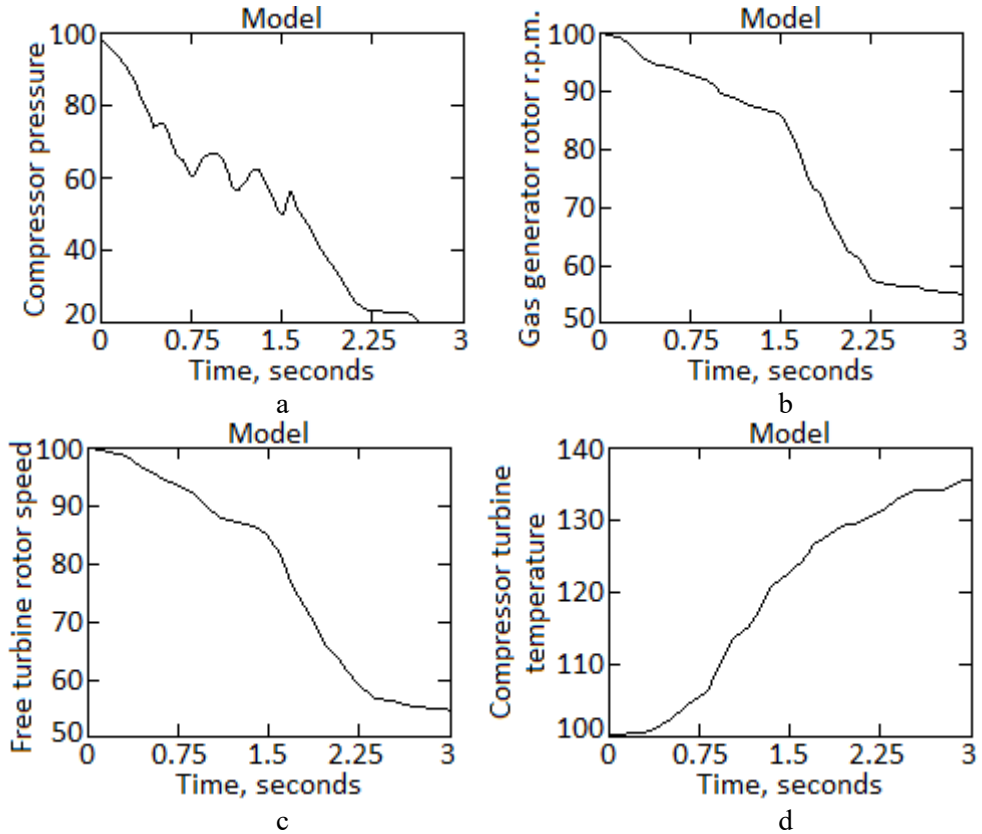


a b c d

**Figure 13**: The resulting diagram of monitoring (diagnostics) of helicopters TE surge by a neural network

The research results displayed in fig. 13 are based on the physical processes occurring in the engine path – using thermogas-dynamic indicators obtained using a universal mathematical model of the engine [30, 31], while taking into account that the surge, as a rule, is accompanied by the following phenomena:

– fluctuations in pressure, velocities and gas flow rates along the path with a pronounced pressure drop downstream of the compressor relative to the pressure at its inlet (fig. 13, a);

– gas generator rotor r.p.m. decrease ($n_{TC}$) (fig. 13, b);

– free turbine rotor rotation frequency decrease ($n_{FT}$) (fig. 13, c);

– gases temperature in front of the compressor turbine increase ($T_G$) (fig. 13, d).

Fig. 13 corresponds to: a – diagram of pressure changes behind the compressor during surge; b – diagram of the dynamics of gas generator rotor r.p.m. during surge; c – diagram of the dynamics of free turbine rotor rotation frequency during surge; d – diagram of changes in gases temperature before the compressor turbine during surging.

According to the results of modeling helicopters TE surge status by a neural network (fig. 13), a division into classes of statuses was carried out [25, 32] (I (red) – surge is present; II (green) – there is no surge; III (blue) – there is a risk of surge), according to the dynamics of changes in the values of engine thermogas-dynamic parameters (Fig. 14).

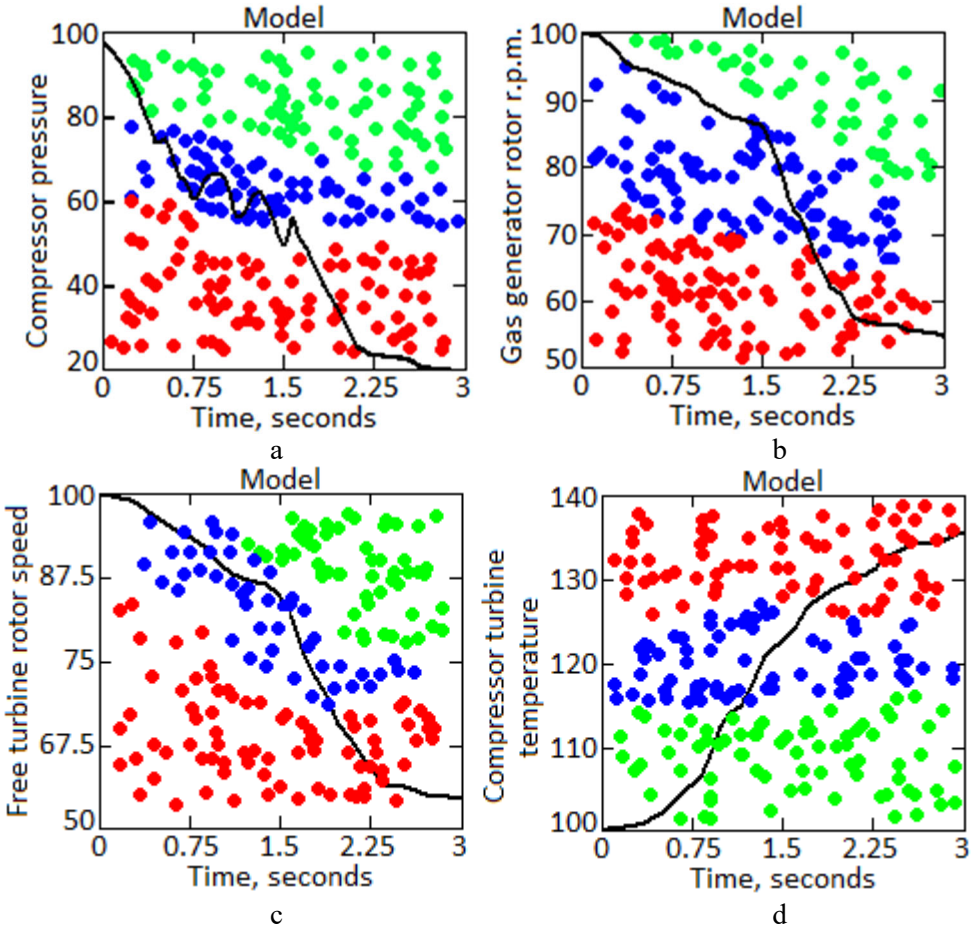


**Figure 14**: The resulting diagram of helicopters TE classification operational status by a neural network

Fig. 14 corresponds to: a – indicator of pressure changes behind the compressor; b – indicator of gas generator rotor r.p.m.; c – indicator of free turbine rotor rotation frequency; d – indicator of gases temperature before the compressor turbine.

A comparative analysis of the accuracy of the classical and neural network methods for diagnostics (monitoring) of helicopters TE (using the TV3-117 engine as an example) pre-surge status is given in table 4 which displays the probabilities of errors of the 1st and 2nd kind [33, 34] when determining the dynamics of changes in engine thermogas-dynamic parameters (according to fig. 13).

**Table 4**
Comparative characteristics of methods

| Method of determination | Probability of error in determining | | | | | | | |
|---|---|---|---|---|---|---|---|---|
| | By parameter $U_C$ | | By parameter $n_{TC}$ | | By parameter $n_{FT}$ | | By parameter $T_G$ | |
| | Type 1st error | Type 2nd error | Type 1st error | Type 2nd error | Type 1st error | Type 2nd error | Type 1st error | Type 2nd error |
| Classic | 1.78 | 1.61 | 1.81 | 1.74 | 2.05 | 1.86 | 1.74 | 1.55 |
| Neural Network | 0.69 | 0.62 | 0.70 | 0.65 | 0.80 | 0.72 | 0.68 | 0.60 |

## 7. Conclusions

1. A mathematical model was further developed that describes the time distribution of pressure in helicopters aircraft turboshaft engines compressor, which, by obtaining a universal expression for determining the distribution of pressure values in the engine compressor, made it possible to develop a neural network method for diagnostics (monitoring) helicopters turboshaft engines pre-surge status in real time.

2. For the first time, a neural network method for diagnostics (monitoring) helicopters turboshaft engines pre-surge status in real time was developed, based on a linear neural network trained using a modified method with direct transmission of information on dynamic neurons, which makes it possible to classify helicopters turboshaft engines statuses in the helicopter flight mode for the presence, absence or risk of surge.

3. The method of training neural networks with direct transmission of information on dynamic neurons was further developed, which, due to the adjustable smoothing parameter from the range from zero to one, made it possible to obtain the predicted output signal value that is closest to the teacher by 99.99 %.

4. It is shown that the errors of the 1st and 2nd kind of the method for diagnostics (monitoring) helicopters turboshaft engines pre-surge status using a linear neural network did not exceed 0.80 % and 0.72 %, respectively, while for the classical method they amounted to 2.05 % and 1.86 %, respectively. The obtained results prove that the application of the developed neural network method will make it 38.77 % more accurate to determine helicopters turboshaft engines current status at helicopter flight mode for the presence or development of surge.

5. The prospect for further research is the implementation of the results of the obtained studies, as well as the developed method for diagnostics (monitoring) helicopters turboshaft engines pre-surge status, into the onboard neural network expert system for integrated monitoring and operation control of helicopters turboshaft engines at helicopter flight mode [35].

The prospects for further research are the integration of this method into self-organizing Kohonen maps, which will improve the method for detecting engine surge using Kohonen self-organizing maps, developed by Viktor Dubrovin and Tetiana Kiprych.

## 8. References


[1] S.-B. Yang, X. Wang, H.-N. Wang, Y.-G. Li, Sliding mode control with system constraints for aircraft engines, ISA Transactions, vol. 98 (2020) 1–10. doi: 10.1016/j.isatra.2019.08.020

[2] W. Jiang, Y. Xu, Z. Chen, N. Zhang, X. Xue, J. Zhou, Measurement of health evolution tendency for aircraft engine using a data-driven method based on multi-scale series reconstruction and adaptive hybrid model, Measurement, vol. 199 (2022) 111502. doi: 10.1016/j.measurement.2022.111502

[3] H. Yu, S. Zhensheng, C. Lijia, Z. Yin, P. Pengfei, Optimization configuration of gas path sensors using a hybrid method based on tabu search artificial bee colony and improved genetic algorithm in turbofan engine, Aerospace Science and Technology, vol. 112 (2021) 106642. doi: 10.1016/j.ast.2021.106642

[4] U. Ahmed, F. Ali, I. Jennions, A review of aircraft auxiliary power unit faults, diagnostics and acoustic measurements, Progress in Aerospace Sciences, vol. 124, no. 1 (2021) 100721. doi: 10.1016/j.paerosci.2021.100721
[5] Y.-Z. Chen, E. Tsoutsanis, C. Wang, L.-F. Gou, A time-series turbofan engine successive fault diagnosis under both steady-state and dynamic conditions, Energy, vol. 263, part D (2023) 125848. doi: 10.1016/j.energy.2022.125848
[6] M. Hruz, P. Pecho, V. Socha, M. Bugaj, Use of the principal component analysis for classification of aircraft components failure conditions using vibrodiagnostics, Transportation Research Procedia, vol. 59 (2021) 166–173. doi: 10.1016/j.trpro.2021.11.108
[7] B. Li, Y.-P. Zhao, Y.-B. Chen, Unilateral alignment transfer neural network for fault diagnosis of aircraft engine, Aerospace Science and Technology, vol. 118 (2021) 107031. doi: 10.1016/j.ast.2021.107031
[8] M. Lungu, R. Lungu, Automatic control of aircraft lateral-directional motion during landing using neural networks and radio-technical subsystems, Neurocomputing, vol. 171 (2016) 471–481 doi: 10.1016/j.neucom.2015.06.084
[9] S. Kiakojoori, K. Khorasani, Dynamic neural networks for gas turbine engine degradation prediction, health monitoring and prognosis, Neural Computing & Applications, vol. 27, no. 8 (2016) 2151–2192. doi: 10.1007/s00521-015-1990-0
[10] S. Pang, Q. Li, H. Zhang, A new online modelling method for aircraft engine state space model, Chinese Journal of Aeronautics, vol. 33, issue 6 (2020) 1756–1773. doi: 10.1016/j.cja.2020.01.011
[11] R. Andoga, L. Fozo, M. Schrotter, M. Ceskovic, Intelligent thermal imaging-based diagnostics of turbojet engines, Applied Sciences, vol. 9, no. 11 (2019) 2253. doi: 10.3390/app9112253
[12] Y. Shmelov, S. Vladov, A. Kryshan, S. Gvozdik, Simulation of transients of gas-parameters flow in compressor of aviation engine TV3-117, Transactions of Kremenchuk Mykhailo Ostrohradskyi National University, issue 4/2018 (111) (2018) 36–42. doi: 10.30929/1995-0519.2018.4.36-42.
[13] G. Coppola, A. Veldman, Global and local conservation of mass, pulse and kinetic energy in the simulation of compressible flow, Journal of Computational Physics, vol. 475 (2023) 111879. doi: 10.1016/j.jcp.2022.111879
[14] J. C. Pozo, V. Vergara, A non-local in time telegraph equation, Nonlinear Analysis, vol. 193 (2020) 111411. doi: 10.1016/j.na.2019.01.001
[15] P. Veigend, G. Necasova, V. Satek, Model of the telegraph line and its numerical solution, Open Computer Science, vol. 8 (2018) 10–17. doi: 10.1515/comp-2018-0002
[16] Y. Shmelov, S. Vladov, Y. Klimova, Simulation gas-dynamic processes occurring in the helicopter engine MI-8MTV, Scientific notes of V.I. Vernadsky Taurida National University. Series: Technical science, vol. 29 (68), no. 2 (2018) 29–34.
[17] M. Adamowicz, G. Zywica, Advanced gas turbines health monitoring systems, Diagnostyka, vol. 19, issue 2 (2018) 77–87. doi: 10.29354/diag/89730
[18] E. Hedrick, K. Hedrick, D. Bhattacharyya, S. E. Zitney, B. Omell, Reinforcement learning for online adaptation of model predictive controllers: Application to a selective catalytic reduction unit, Computers & Chemical Engineering, vol. 160 (2022) 107727 doi: 10.1016/j.compchemeng.2022.107727
[19] R. Vang-Mata, Multilayer Perceptrons: Theory and Applications, New York, Nova Science Publishers (2020) 143.
[20] A. Sarraf, S. Khalili, An upper bound on the variance of scalar multilayer perceptrons for log-concave distributions, Neurocomputing, vol. 488, no. 1 (2022) 540–546. doi: 10.1016/j.neucom.2021.11.062
[21] W. Mlynarski, M. Hledik, T. R. Sokolowski, G. Tkacik, Statistical analysis and optimality of neural systems, Neuron, vol. 109, issue 7 (2021) 1227–1241.e5 doi: doi.org/10.1016/j.neuron.2021.01.020
[22] C. Qin, J. Wang, H. Zhu, J. Zhang, S. Hu, D. Zhang, Neural network-based safe optimal robust control for affine nonlinear systems with unmatched disturbances, Neurocomputing, vol. 506 (2022) 228–239. doi: doi.org/10.1016/j.neucom.2022.07.072
[23] T. Chepenko, Time series predicting methods based on artificial neural networks with time delay elements, Kharkiv National University of Radio Electronics. URL: https://openarchive.nure.ua/server/api/core/bitstreams/dd87fbf2-2b7c-49b8-bf6e-ad2beee80361/content
[24] S. Vladov, Y. Shmelov, R. Yakovliev, Optimization of Helicopters Aircraft Engine Working Process Using Neural Networks Technologies. COLINS-2022: 6th International Conference on

Computational Linguistics and Intelligent Systems, May, 12–13, 2022, Gliwice, Poland. CEUR Workshop Proceedings (ISSN 1613-0073), vol. 3171 (2022) 1639–1656.
[25] S. Vladov, Y. Shmelov, R. Yakovliev, Methodology for Control of Helicopters Aircraft Engines Technical State in Flight Modes Using Neural Networks, The Fifth International Workshop on Computer Modeling and Intelligent Systems (CMIS-2022), May, 12, 2022, Zaporizhzhia, Ukraine, CEUR Workshop Proceedings (ISSN 1613-0073) vol. 3137 (2022) 108–125. doi: 10.32782/cmis/3137-10
[26] S. Vladov, Y. Shmelov, R. Yakovliev, Modified Helicopters Turboshaft Engines Neural Network On-board Automatic Control System Using the Adaptive Control Method. ITTAP'2022: 2nd International Workshop on Information Technologies: Theoretical and Applied Problems, November 22–24, 2022, Ternopil, Ukraine. CEUR Workshop Proceedings (ISSN 1613-0073), vol. 3309 (2022) 205–229.
[27] H.-Y. Kim, Statistical notes for clinical researchers: Chi-squared test and Fisher's exact test, Restor Dent Endod, vol. 42, no. 2 (2017) 152–155. doi: 10.5395/rde.2017.42.2.152
[28] H. Mark, J. Workman Jr., Chapter 65 – Linearity in Calibration, Act III Scene II: A Discussion of the Durbin-Watson Statistic, a Step in the Right Direction, Chemometrics in Spectroscopy (Second Edition), (2018) 433–440. doi: 10.1016/B978-0-12-805309-6.00065-9
[29] P. Carpena, A. V. Coronado, On the Autocorrelation Function of 1/f Noises, Mathematics, vol. 10 (2022) 1416. doi: 10.3390/math10091416
[30] O. Avrunin, S. Vladov, M. Petchenko, V. Semenets, V. Tatarinov, H. Telnova, V. Filatov, Y. Shmelov and N. Shushlyapina. Intelligent automation systems, Kremenchuk, Novabook (2021) 322. doi: 10.30837/978-617-639-347-4
[31] S. Pang, Q. Li, B. Ni, Improved nonlinear MPC for aircraft gas turbine engine based on semi-alternative optimization strategy, Aerospace Science and Technology, vol. 118 (2021) 106983. doi: 10.1016/j.ast.2021.106983
[32] L. Zhao, S. H. Goh, Y. H. Chan, B. L. Yeoh, H. Hu, M. H. Thor, A. Tan, J. Lam, Optimization of an Artificial Neural Network System for the Prediction of Failure Analysis Success, Microelectronics Reliability, vol. 92 (2019) 136–142. doi: 10.1016/j.microrel.2018.11.014
[33] J. Park, H. E. Kim, I. Jang, Empirical estimation of human error probabilities based on the complexity of proceduralized tasks in an analog environment, Nuclear Engineering and Technology, vol. 54, issue 6 (2022) 2037–2047. doi: 10.1016/j.net.2021.12.025
[34] A. Silva, M. Gouvea, Study on the effect of sample size on type I error, in the first, second and first-two digits excessmad tests, International Journal of Accounting Information Systems, vol. 48 (2023) 100599. doi: 10.1016/j.accinf.2022.100599
[35] Y. Shmelov, S. Vladov, Y. Klimova, M. Kirukhina, Expert system for identification of the technical state of the aircraft engine TV3-117 in flight modes, System Analysis & Intelligent Computing: IEEE First International Conference on System Analysis & Intelligent Computing (SAIC), 08–12 October 2018. 77–82. doi: 10.1109/SAIC.2018.8516864